Structural Engineering and Mechanics, *Vol. 67, No. 3 (2018) 255-265*
DOI: https://doi.org/10.12989/sem.2018.67.3.255

Prestress force effect on fundamental frequency and deflection shape of PCI beams

Marco Bonopera[*1,4], Kuo-Chun Chang[2a], Chun-Chung Chen[1b], Yu-Chi Sung[1,3c] and Nerio Tullini[4d]

[1]*Bridge Engineering Division, National Center for Research on Earthquake Engineering, Taipei, Taiwan*
[2]*Department of Civil Engineering, National Taiwan University, Taipei, Taiwan*
[3]*Department of Civil Engineering, National Taipei University of Technology, Taipei, Taiwan*
[4]*Department of Engineering, University of Ferrara, Ferrara, Italy*

(Received February 27, 2018, Revised May 14, 2018, Accepted May 17, 2018)

Abstract. The prestress force effect on the fundamental frequency and deflection shape of Prestressed Concrete I (PCI) beams was studied in this paper. Currently, due to the conflicts among existing theories, the analytical solution for properly considering the structural behavior of these prestressed members is not clear. A series of experiments were conducted on a large-scale PCI beam of high strength concrete with an eccentric straight unbonded tendon. Specifically, the simply supported PCI beam was subjected to free vibration and three-point bending tests with different prestress forces. Subsequently, the experimental data were compared with analytical results based on the Euler-Bernoulli beam theory. It was proved that the fundamental frequency of PCI beams is unaffected by the increasing applied prestress force, if the variation of the initial elastic modulus of concrete with time is considered. Vice versa, the relationship between the deflection shape and prestress force is well described by the magnification factor formula of the compression-softening theory assuming the secant elastic modulus.

Keywords: compression-softening theory; deflection shape; fundamental frequency; PCI beam; prestress force

1. Introduction

The stiffness of prestressed concrete beams is a crucial parameter defining, for example, the bridge deflection. Vibration measurements taken during the operation stage of a bridge are useful methods to evaluate the stiffness of prestressed concrete beams. Thus, questions arise on how the dynamic response of these beams is affected by the applied prestress force. This argument was discussed extensively, e.g., in the literature review by Noble *et al*. (2015, 2016). Several works (Miyamoto *et al*. 2000, Law and Lu 2005, Lu and Law 2006, Bonopera *et al.* 2018a, b, c) assumed that the prestress force in the tendon is equivalent to an external axial load assigned to the beam ends. Consequently, the natural frequencies of prestressed members tend to decrease as the compressive force is increased. This is known as the compression-softening effect and occurs in externally axially loaded Euler-Bernoulli beams prone to buckling failure (Timoshenko and Gere 1961, Bazant and Cedolin 1991). Nonetheless, several dynamic tests illustrated an increase of natural frequencies with an increase in prestress force (Hop 1991, Saiidi *et al*. 1994, Kim *et al*. 2004, Zhang and Li 2007), as occurs in tension members within the elastic range (Tullini and Laudiero 2008, Tullini *et al*. 2012, Rebecchi *et al*. 2013), thus contradicting the compression-softening theory. Noh *et al*. (2015) and Li and Zhang (2016) suggested that flexural rigidity (and natural frequency) of concrete beams with an eccentric straight unbonded tendon is also increased by other parameters, such as the beam camber, geometric stiffness of the cable and the stiffening effect of the beam-tendon system. Hamed and Frostig (2006) and Wang *et al*. (2013) suggested that natural frequencies of prestressed members with an eccentric straight tendon are unaffected by the prestress force. Instead, Jaiswal (2008) pointed out that the increase of beam's flexural rigidity depends on the eccentricity of the straight unbonded tendon, thus inducing greater moment and stiffening effect in the element. They claimed that the prestress force in the tendon modifies its original line of action during the member vibration, thus preserving its eccentricity with respect to the beam axis. Accordingly, a prestress force does not cause Euler buckling to occur. Because of the conflicts among the above theories, it results no clear which is the reference model for properly considering the dynamic behavior of concrete members with a straight unbonded tendon. Moreover, the aforementioned references lack of experimental studies on the relationship between the prestress force and natural frequency in large-scale concrete beams. In short, experiments on small-scale prestressed concrete members were executed only. Proper information on the structural

*Corresponding author, Ph.D.
E-mail: bonopera@ncree.narl.org.tw or marco.bonopera@unife.it
[a]Professor
E-mail: ciekuo@ntu.edu.tw
[b]Ph.D.
E-mail: ccchen@ncree.narl.org.tw
[c]Professor
E-mail: sungyc@ntut.edu.tw
[d]Professor
E-mail: nerio.tullini@unife.it

http://www.techno-press.com/journals/sem&subpage=7
ISSN: 1225-4568 (Print), 1598-6217 (Online)

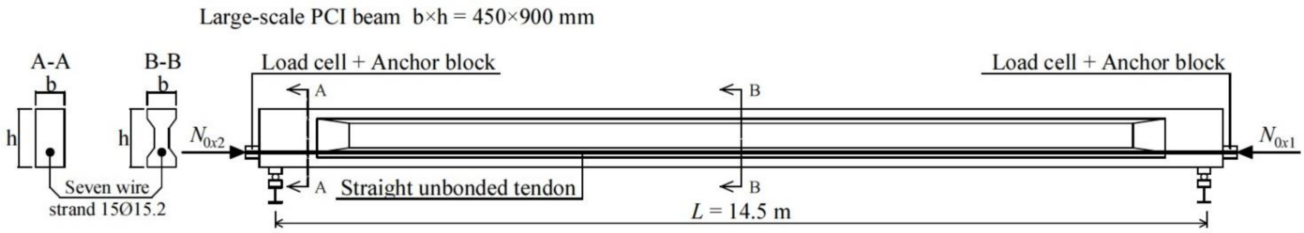

Fig. 1 Large-scale PCI beam with an eccentric straight unbonded tendon

behavior of prestressed concrete beams are also required to study the prestress loss phenomena (Ortega *et al.* 2018, Bonopera *et al.* 2018c).

In this study, due to the conflicts among the aforementioned theories, a large-scale simply supported Prestressed Concrete I (PCI) beam with an eccentric straight unbonded tendon and high strength concrete was adopted. The aim was to find the proper analytical solution to be taken into consideration for the dynamic and static behavior of a typical prestressed member. Free vibration and three-point bending tests with different prestress forces were performed on the beam in distinct days, therefore under different curing conditions of concrete. A set of servo velocity seismometers and Linear Variable Differential Transformers (LVDTs) were installed along the PCI beam's length to measure the fundamental frequency and deflection shape. The member was found to be always preserved against crack formation. Subsequently, the results of numerical modeling based on the Euler-Bernoulli beam theory, where the cross sectional second moment of the area corresponded to the composite section formed of concrete and tendon, were compared with the experimental data. Specifically, the reference model was a simply supported Euler-Bernoulli beam prestressed by an eccentric straight unbonded tendon, where the prestress force was considered as an external compressive load applied to the beam ends. Results indicated that experimental data can be simulated analytically, thus demonstrating the accuracy of the assumption of the beam's mechanical model, as predicted using the dynamic and static theory. The experimental natural frequencies were well described by the formula for the free vibration of the simply supported Euler-Bernoulli beam (Young and Budynas 2002), as predicted using the first-order theory. Thus, the fundamental frequency of PCI beams with an eccentric straight unbonded tendon is unaffected by the prestress force if the variation of the initial elastic modulus of concrete with time, due to its early curing process, is considered. Vice versa, the deflection shape is well approximated by the magnification factor formula of the compression-softening theory (Timoshenko and Gere 1961, Bazant and Cedolin 1991) assuming the secant elastic modulus.

2. Large-scale laboratory testing program

2.1 PCI beam with an eccentric straight unbonded tendon and related test layout

A large-scale PCI beam of b = 450 mm in width, h = 900 mm in height and high strength concrete was adopted (Fig. 1). The beam was longitudinally reinforced with rebars and transversally with stirrups, according to the Building Code Requirements for Structural Concrete (ACI 318-14), corresponding to an unit weight of steel ρ_s of approximately 1.23 kN/m^3. The straight unbonded tendon had an eccentricity of e = 220 mm (e / h = 0.24) with respect to the centroid of the cross section. Specifically, the tendon was composed by 15 steel cables "seven wire strand" of 15.2 mm in diameter inserted into a metallic duct embedded along the concrete beam's length (Fig. 1). The metallic duct was not injected. The ultimate yield strength and elastic modulus of steel cables were respectively of 1860 MPa and 200 GPa. Two pinned-end supports were placed at the beam ends to reproduce the most common boundary conditions of concrete beams, resulting a clear span of L = 14.5 m (Fig. 1). The cross sectional second moment of the area of the PCI beam's composite section $I_{exact} = 2.696 \times 10^{10}$ mm^4. The corresponding cross sectional area $A_{exact} = 2.981 \times 10^5$ mm^2. The slenderness ratio was equal to 49. The beam had a rectangular cross section, of b × h = 450 mm × 900 mm, for a length of 650 mm from the pinned-end supports. The cross sectional area of the eccentric straight tendon $A_{tendon} = 2.085 \times 10^3$ mm^2. The geometric dimensions were verified by measuring-systems of 0.01-mm tolerance (laser rangefinder and caliper), once the member was positioned on the supports. The elastic modulus of the used high strength concrete was evaluated through compression tests on cylinders after 28-days of curing and during the experimental period (Section 2.4).

The PCI beam was inserted in a test rig (Fig. 2(a)). At one beam end, a hydraulic oil jack, of 4000 kN-force capacity, was used to apply the prestress forces pulling the tendon outward. At both ends, respectively, a 4000 kN load cell, with accuracy of 2 mV/V, was placed to measure the assigned prestress forces N_{0x1} and N_{0x2} (Fig. 3(b)). Four prestress forces $N_{0x,aver}$ were totally applied by values of approximately 1563, 1722, 1819 and 1921 kN to induce small second-order effects. A difference of approximately 100 kN between the prestress forces $N_{0x,aver}$ was firstly planned. The indoor safety conditions of the laboratory involved the higher prestress force ($N_{0x,aver}$ = 1921 kN) to be lower than 2000 kN. Thus, the maximum tensile strength, reached in the tendon, was of approximately 50% of the ultimate yield strength of the cables. The different prestress forces N_{0x1} and N_{0x2}, measured at the beam ends, were caused by the friction losses along the tendon (Fig. 1). The measure systems included four servo velocity seismometers and eight LVDTs deployed along the beam's length (Fig. 4). The arrangement of the various devices is described as

(a) (b)

Fig. 2(a) Indoor test rig. (b) LVDTs along the PCI beam’s length

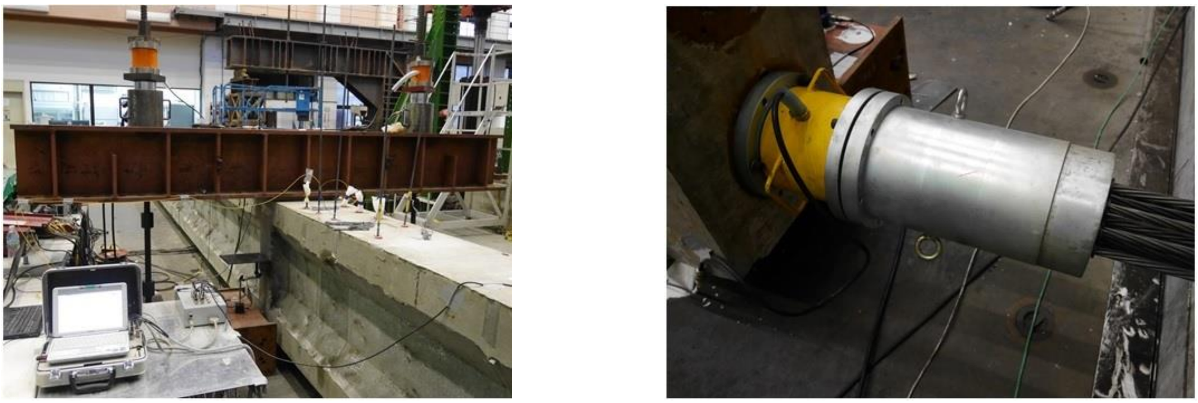

(a) (b)

Fig. 3(a) Transverse steel beam at the midspan of the PCI beam and acceleration data logger. (b) Load cell, steel transition part and steel circular plate at one beam end

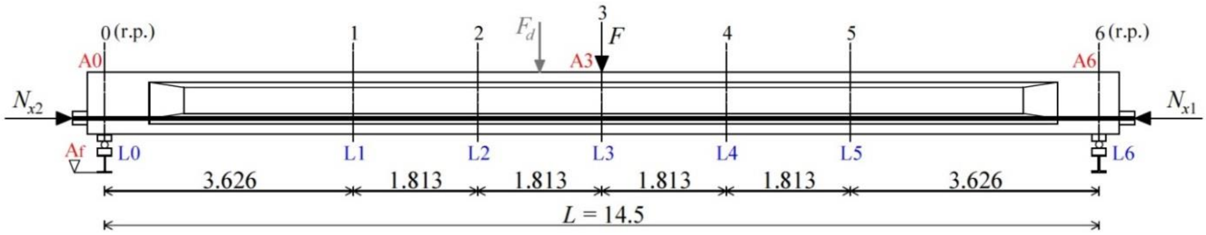

Fig. 4 Test layout with locations of the instrumented sections with velocity seismometers and LVDTs. Units: m

follows:

Servo velocity seismometer: Four high-precision servo velocity seismometers, VSE-15D, manufactured by Tokyo Sokushin Co. Ltd., were chosen for the experiments. The servo velocity seismometers have a sensitivity of 5 mV/gal and are lightweight (270 g). One velocity seismometer, labeled A3, was vertically placed on the top of the PCI beam, corresponding to the midspan cross section (i = 3), to collect acceleration data with respect to the strong axis (Fig. 4). Two velocity seismometers, labeled A0 and A6, were instead fixed at the beam ends (i = 0 and 6). Additionally, one reference velocity seismometer, labeled Af, was fixed to the floor, close to the beam end at i = 0, to check possible abnormalities of the sensing system. All sensors were connected to a signal conditioner and, subsequently, to a data logger located on a desk close to the test rig (Fig. 3(a)). The test layout in Fig. 4 shows their positions (in red).

Linear variable differential transformer (LVDT): Eight LVDTs, of 0.002-mm tolerance, were positioned at the cross sections i = 0, ..., 6 (Fig. 4). Steel plates were used to locate each LVDT probe at the level of the beam axis (Fig. 2(b)). Specifically, two reference LVDTs, labeled L0 and L6, were fixed at the beam ends i = 0 and 6, forming the reference line for the measurement system between the boundary conditions. An additional LVDT was located on the opposite side of the midspan cross section at i = 3, to measure possible rotations along the member axis. All LVDTs were connected to a data logger positioned on a

(a) (b)

Fig. 5(a) Arrangement of the hydraulic oil jack on one steel rebar anchored close to the midspan. (b) Arrangement of the hydraulic pump connected to the hydraulic oil jack before activation

Table 1 Measured loading parameters

Days of concrete curing	N_{0x2} (kN)	N_{0x1} (kN)	$N_{0x,aver}$ (kN)	N_{x2} (kN)	N_{x1} (kN)	$N_{x,aver}$ (kN)	F (kN)	v_1 (mm)	v_2 (mm)	v_3 (mm)	v_4 (mm)	v_5 (mm)
	1514	1614	1564	1524	1620	1572	80.5	3.68	4.85	5.29	4.80	3.59
87	1514	1614	1564	1526	1622	1574	100.9	4.58	6.08	6.67	6.03	4.47
	1520	1613	1567	1529	1624	1577	139.7	6.26	8.35	9.21	8.34	6.25
	1668	1775	1722	1678	1789	1733	160.3	7.29	9.64	10.56	9.60	7.37
88	1668	1775	1722	1679	1790	1735	171.4	7.85	10.40	11.42	10.36	7.93
	1668	1775	1722	1681	1792	1737	182.4	8.43	11.20	12.31	11.14	8.51
	1754	1882	1818	1776	1896	1836	179.8	8.13	10.77	11.84	10.73	8.18
88	1764	1880	1822	1775	1895	1835	180.7	8.16	10.81	11.86	10.79	8.24
	1754	1882	1818	1779	1898	1838	196.8	9.06	12.05	13.30	12.00	9.10
	1848	1989	1918	1872	2002	1937	190.2	8.52	11.26	12.37	11.18	8.51
90	1859	1987	1923	1871	2002	1937	191.8	8.68	11.48	12.55	11.44	8.77
	1848	1989	1918	1876	2006	1941	210.6	9.64	12.80	14.10	12.71	9.61

desk close to the test rig. The test layout in Fig. 4 shows the positions of the LVDTs (in blue). Fiber Bragg grating-differential settlement measurement (FBG-DSM) sensors (the green pillars in Fig. 2(b)) were used in a different study and the corresponding measurements were not taken into account in this work.

2.2 Free vibration testing

Free vibration tests were performed after the application of prestress forces $N_{0x,aver}$. Specifically, four test cases with $N_{0x,aver}$ equal to 1563, 1722, 1819 and 1921 kN were considered (Fig. 1). All velocity seismometers (Section 2.1) acquired the acceleration data at a sampling rate of 200 Hz and with a block size of 2048 samples. For every prestress force $N_{0x,aver}$, vibration measurements were performed thrice, for a total of twelve experiments. In detail, free vibrations were always imposed by breaking a steel rebar of 10 mm in diameter anchored close to the midspan of the beam (Fig. 5(a)). The ultimate strength f_{sk} of 540 MPa of the rebar was reached using a hydraulic oil jack, of 100 kN-force capacity, pulling up each rebar until rupture (Fig. 5(a)). The hydraulic oil jack was actuated by a hydraulic pump of 96.53 MPa in maximum pressure capacity, positioned on the floor (Fig. 5(b)). Thus, the concrete beam was vertically excited by a release force F_d of approximately 42.4 kN (Fig. 4) and its dynamic response was measured along the strong axis. The large-scale PCI beam did not develop cracks during testing. The applied prestress forces N_{0x1} and N_{0x2} (Fig. 1) were recorded every second for nearly 200 seconds by a data acquisition unit and using a distinct data log. The average measurements N_{0x1} and N_{0x2} for every test case are illustrated in Section 3.2.

2.3 Three-point bending tests

After free vibration measurements, as described in the previous section, an additional load F was applied by a transverse steel beam at the midspan of the PCI beam for every prestress force $N_{0x,aver}$ (Fig. 3(a)). The vertical load F was increased from its initial magnitude, then gradually to two different values, depending on the magnitude of the prestress force $N_{0x,ave}$. After the application of every load F, prestress forces $N_{0x,aver}$ always experienced a small increment. The average measurements of initial prestress forces (N_{0x2}, N_{0x1}, $N_{0x,aver}$), prestress forces (N_{x2}, N_{x1}, $N_{x,aver}$) when loads F were applied, loads F and deflections v_i for one repetition of the test combinations are listed in Table 1. The load F was always pulled both up and down using two hydraulic oil jacks, of 1000 kN-force capacity, fixed to the floor, and two other hydraulic oil jacks, similarly of 1000 kN-force capacity, fastened at the top of the steel beam (Fig. 3(a)). All values of the applied force F were obtained by summing the measurements of two load cells, of 1000 kN-force capacity and 2 mV/V accuracy, located between the upper oil jacks and two steel plates (Fig. 3(a) and Table 1). This test condition was repeated thrice for every point load F, resulting in thirty-six tests, totally.

The displacements v_i, for i = 1, ..., 5, located according to the layout shown in Fig. 4, were recorded by the LVDTs after applying every load F. The initial reference deflection shape corresponded to that one after the assignment of prestress forces N_{0x1} and N_{0x2} (Fig. 6). Every prestress force $N_{x,aver}$ prevented the PCI beam from developing cracks under the vertical load F. All test measurements were

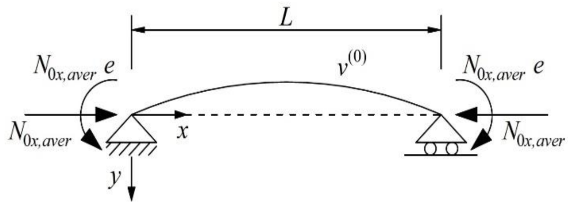

Fig. 6 Reference model for the PCI beam. Deflection shape $v^{(0)}$ after eccentric prestress force $N_{0x,aver}$ has been applied. The dashed line represents the configuration of the beam without any imposed load

recorded every second for nearly 200 seconds using a data acquisition unit.

2.4 Evaluation of the time-dependent elastic modulus of the high strength concrete

A set of 100 mm × 200 mm concrete cylinders were cast to measure the time-dependent elastic modulus of the high strength concrete through compression tests. Portland cement ASTM type I, chemical admixture, steel slag powder and a Class F fine fly ash were used in concrete making. The PCI beam and all cylindrical specimens were maintained under the same curing environmental conditions after casting and, specifically, outdoor the laboratory spaces. The elastic modulus E of each single cylinder was estimated using Eq. (1), in accordance with the ASTM C 469/C 469M-14 Standard (Annual Book of ASTM Standards 2016)

$$E = E_{fvt} = \frac{\sigma_2 - \sigma_1}{\varepsilon_2 - 0.00005} \tag{1}$$

where σ_2 is the stress corresponding to the 40% of the characteristic strength of concrete f_{ck}, and σ_1 is the stress corresponding to the longitudinal strain of 0.00005. ε_2 is the longitudinal strain produced by σ_2.

The aforementioned three values were determined by the "longitudinal compressive stress *vs*. longitudinal strain" graphs of the single cylinders, where the elastic modulus E was the initial tangent value. One compressometer, equipped with two LVDTs, was used as strain measurement system. The universal testing machine was set at a loading rate of approximately 1 mm/min.

By considering the small second-order effects imposed during free vibration testing (Sections 2.2), an additional value of the initial tangent elastic modulus, labeled E_{fvt}, was determinated using Eq. (1) for every cylinder where, conversely, σ_2 is the existing maximum stress in the PCI beam during testing and corresponding to the day of curing under observation. Similarly, σ_1 is the stress corresponding to the longitudinal strain of 0.00005, whereas ε_2 is the longitudinal strain produced by the maximum stress σ_2. In this way, a more realistic investigation of the elastic modulus of the PCI beam was obtained. A Finite Element (FE) second-order static analysis that assumed 9 beam elements and the cross sectional second moment of the area I_{exact} (Fig. 1) was used to compute the maximum stress σ_2 during each day of free vibration testing by applying the

Table 2 Measured unit weight ρ_c, characteristic strength f_{ck}, stress σ_2 and elastic modulus E of the high strength concrete

					Eq. (1) with $\sigma_2 = 0.4\,f_{ck}$				Eq. (1) with max stress σ_2			
Days of concrete curing	$N_{0x,aver}$ (kN)	Cyl.	ρ_c (kN/m^3)	f_{ck} (MPa)	σ_2 (MPa)	E (MPa)	E_{aver} (MPa)	Var. (%)	σ_2 (MPa)	E_{fvt} (MPa)	$E_{fvt,aver}$ (MPa)	Var. (%)
28	–	A	–	84.80	33.92	37458	36490	–	–	–	–	–
		B	–	94.28	37.71	34752			–	–		
		C	–	93.43	37.37	37365			–	–		
		D	–	82.70	33.08	36384			–	–		
87	1563	1	24.17	98.25	39.30	36061	37139	1.8	8.25	40053	40163	10.1
		2	24.39	113.82	45.53	37712			8.25	41515		
		3	24.89	98.30	39.32	38669			8.25	40854		
		4	24.07	98.20	39.28	36112			8.25	38230		
88	1722	1	24.14	100.59	40.24	36627	37050	1.5	8.79	38350	39609	8.5
		2	24.11	86.52	34.61	35253			8.79	40244		
		3	24.39	104.34	41.74	38108			8.79	40133		
		4	23.68	107.28	42.91	38211			8.79	39709		
88	1819	1	24.14	100.59	40.24	36627	37050	1.5	9.11	38281	39598	8.5
		2	24.11	86.52	34.61	35253			9.11	40213		
		3	24.39	104.34	41.74	38108			9.11	40274		
		4	23.68	107.28	42.91	38211			9.11	39623		
90	1921	1	24.35	114.78	45.91	38080	37425	2.6	12.45	39782	39758	9.0
		2	24.38	104.62	41.85	36769			12.45	39733		

corresponding prestress force $N_{0x,aver}$.

The measured elastic modulus E after 28-days and during the experimental testing period are summarized in Table 2. Specifically, the average elastic moduli E_{aver} and $E_{fvt,aver}$ were obtained for each day by testing four cylinders. Separately, two specimens were tested at 90-days of curing. The variation of the elastic modulus E_{aver} experienced a progressive increment of 1.8%, 1.5% and 2.6% with respect to the value gained after 28-days, whereas the variation of the elastic modulus $E_{fvt,aver}$ experienced a progressive increment of 10.1%, 8.5% and 9.0%, respectively. Thus, the average reference elastic moduli were E_{ref} = 37166 MPa and $E_{fvt,ref}$ = 39782 MPa. The higher values of the elastic modulus $E_{fvt,aver}$ were caused by the lower stresses σ_2 assumed in Eq. (1), as reported in Table 2. The average characteristic strength of the high strength concrete f_{ck} was 102 MPa, considering the compression tests at 87-, 88- and 90-days of curing (Table 2). The experimental unit weight of concrete, ρ_c = 24.21 kN/m^3, was obtained by the average of the values of each cylinder shown in Table 2. Notably, the large difference between the characteristic strengths f_{ck} at 88- and 90-days of curing (Table 2) was probably caused by the different steel slag powder and fly ash contents in the concrete mixtures of the cylinders (Haque and Kayali 1998, Palanisamy *et al.* 2015).

3. Prestress force effect on the fundamental frequency based on the free vibration testing

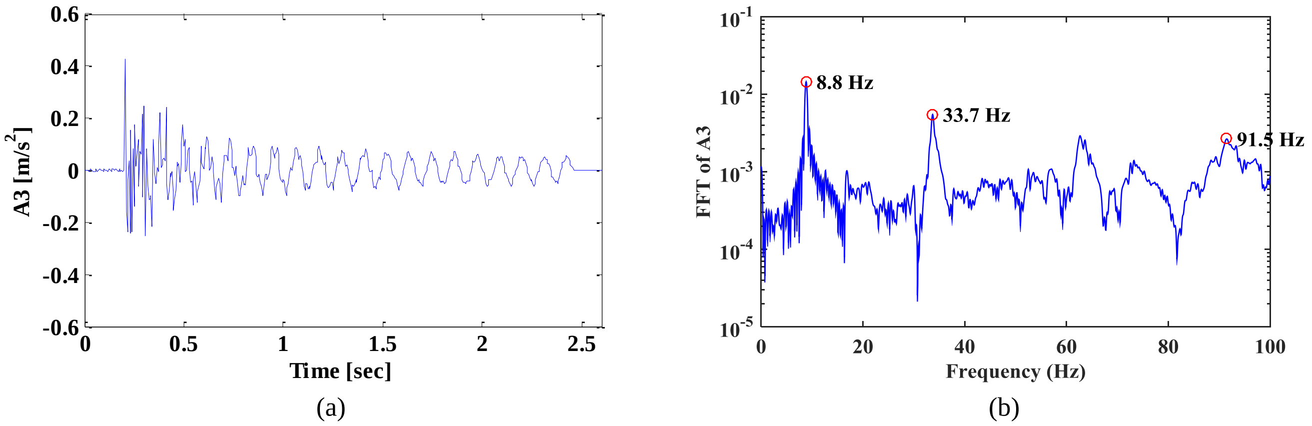

Fig. 7(a) Acceleration time history and (b) FFT for the instrumented section A3 when $N_{0x,aver}$ = 1563 kN

Table 3 Comparison of the experimental and analytical values of the fundamental frequency f_I

						f_I with E_{aver}			f_I with $E_{fvt,aver}$	
Days of concrete curing	N_{0x2} (kN)	N_{0x1} (kN)	$N_{0x,aver}$ (kN)	f_I Exp (Hz)	E_{aver} (MPa)	f_I Eq. (2) (Hz)	f_I Eq. (3) (Hz)	$E_{fvt,aver}$ (MPa)	f_I Eq. (2) (Hz)	f_I Eq. (3) (Hz)
87	1515	1611	1563	8.8 –	37139	8.4 -4.5%	8.5 -3.4%	40163	8.7 -1.1%	8.8 0.0%
88	1668	1775	1722	8.8 –	37050	8.3 -5.7%	8.5 -3.4%	39609	8.6 -2.3%	8.8 0.0%
88	1757	1882	1819	8.8 –	37050	8.3 -5.7%	8.5 -3.4%	39598	8.6 -2.3%	8.8 0.0%
90	1854	1988	1921	8.9 –	37425	8.3 -6.7%	8.5 -4.5%	39758	8.6 -3.4%	8.8 -1.1%

3.1 Analytical model

A simply supported Euler-Bernoulli beam was adopted as reference model (Fig. 6). The cross sectional area A_{exact} and the second moment of the area I_{exact} were established in accordance with the design drawings and, specifically, considering the composite behavior of the PCI beam's cross section formed of concrete and cable. The elastic modulus of concrete was assumed to be a known parameter. When the compression-oftening theory is considered, the prismatic concrete member is subjected to an eccentric prestress force $N_{0x,aver}$ (with eccentricity e) with respect to the centroid of the cross section (Fig. 6). The prestress force $N_{0x,aver}$ is considered externally applied as a compressive axial load (Fig. 6). The deflection shape, after the eccentric prestress force $N_{0x,aver}$ has been applied, is labeled as $v^{(0)}$ in Fig. 6. By assuming the characteristic strength of concrete, f_{ck} = 102 MPa (Section 2.4), the serviceability limit state in the PCI beam is satisfied until a prestress force of 4300 kN, corresponding to 9.1% of the Euler buckling load N_{crE} = $\pi^2 E_{ref} I_{exact}/L^2$ = 47036 kN.

3.2 Free vibration tests and comparison with analytical model

Fig. 7(a) shows the acceleration measured at the midspan cross section (i = 3) (Fig. 4), whereas Fig. 7(b) reports the corresponding Fast Fourier Transform (FFT). The peak-picking method was adopted. In short, natural frequencies were located at each peak of the FFT functions (Fig. 7(b)). In total, twelve FFT functions were collected, considering that every test was repeated thrice for every prestress force $N_{0x,aver}$. The maximum prestress force $N_{0x,aver,max}$ = 1921 kN was of approximately 45% of the maximum allowable prestress force of 4300 kN.

The average fundamental frequencies f_I, from the three repetitions, are listed in Table 3. Notably, the velocity seismometer A3 always provided equal frequency during the repetitions of each test case. The average measurements N_{0x2} and N_{0x1} (recorded for nearly 200 seconds by a data acquisition unit) are also reported in Table 3.

Based on the compression-softening model, the fundamental frequency of an externally axially loaded, simply supported beam (Fig. 6) is (Young and Budynas 2002)

$$f_I = \frac{\pi}{2}\sqrt{\frac{EI_{exact}\,g}{m_{tot}L^4}}\sqrt{1-\frac{N_{0x,aver}}{N_{crE}}} \tag{2}$$

where the PCI beam's weight per unit length is $m_{tot} = (\rho_s + \rho_c) \times A_{exact}$ = 7.584 kN/m. The elastic modulus of each test day, labeled as E and dependent on the curing of concrete, have to be assumed in the calculations by the values of E_{aver} or $E_{fvt,aver}$ (Table 2). The cross sectional second moment of the area of the composite section I_{exact} was considered in accordance with the design drawings. Moreover, Euler buckling load of the PCI beam is obtained by N_{crE} = $\pi^2 EI_{exact}/L^2$, where the elastic modulus E takes the values of E_{aver} or $E_{fvt,aver}$ for each test day (Table 2). The gravitational acceleration g is 9.81 m/s^2. By neglecting the term containing the compressive axial load $N_{0x,aver}$, the fundamental frequency f_I reduces to

$$f_I = \frac{\pi}{2}\left(\frac{EI_{exact}\,g}{m_{tot}L^4}\right)^{1/2}. \tag{3}$$

Table 3 points out the effect of the prestress force $N_{0x,aver}$ on the fundamental frequency. Notably, the experimental frequency increased from 8.8 Hz to 8.9 Hz despite the increasing of 22.9% of the corresponding average prestress

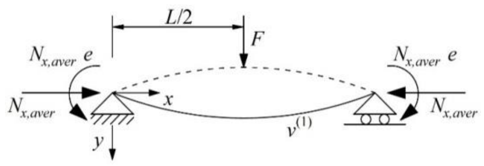

Fig. 8 Reference model of the PCI beam. Deflection curve $v^{(1)}$ after load F has been applied to the deflection curve $v^{(0)}$ depicted in Fig. 6. The dashed line represents the initial deflection curve

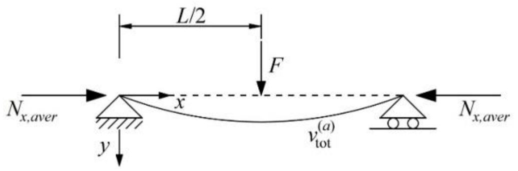

Fig. 9 Reference model of the PCI beam. Deflection curve $v_{\mathrm{tot}}^{(a)}$ after load F has been applied. The dashed line represents the initial deflection curve

force $N_{0x,aver}$. Conversely, the increase of the elastic modulus E_{aver} was 37425/37139 = 1.01, corresponding to an increase of 0.8% of the square root of E_{aver} with time; whereas, the variation of the elastic modulus $E_{fvt,aver}$ (39758/40163 = 0.99) can be neglected. Therefore, the increase of the fundamental frequency seems to be related to the increase of the square root of the elastic modulus of concrete with time. This trend confirms the theoretical results presented by Hamed and Frostig (2006), Jaiswal (2008) and Wang *et al*. (2013), where natural frequencies of prestressed concrete beams with a straight unbonded tendon are unaffected by the prestress force. Notably, other previous studies (Saiidi *et al*. 1994, Jacobs and De Roeck 2003, Limongelli *et al*. 2016) agree with the results illustrated in Table 3.

Table 3 compares the mean values of the fundamental frequency of the PCI beam with the corresponding analytical values f_I obtained by Eqs. (2)-(3), that respectively use the values E_{aver} and $E_{fvt,aver}$. The beam model based on the first-order theory (Eq. (3)) can properly represent the dynamic behavior of the PCI beam. In fact, a maximum error of 1.1% was obtained by considering the elastic modulus $E_{fvt,aver}$, even though the prestress force was increased of 23%, from $N_{0x,aver,min}$ = 1563 kN to $N_{0x,aver,max}$ = 1921 kN, which is equal to 4.1% of N_{crE}. The relative errors increase by adopting the compression-softening theory (Eq. (2)). Notably, the cables (under tensile force) were always in contact with the surrounding metallic duct during testing. Thus, the beam model that uses the first-order theory (Young and Budynas 2002) can well describe the dynamic behavior of PCI beams with an eccentric straight unbonded tendon.

A FE analysis that assumed 9 beam elements and the flexural rigidity variation along the PCI beam's length (Fig. 1) pointed out that the fundamental frequency does not vary with respect to the analytical models (Eqs. (2)-(3)). Nine Euler-Bernoulli beam elements adopting exact shape functions describing second-order effects (Bazant and Cedolin 1991) were used to consider the compression-softening theory. The reference value $E_{fvt,ref}$ = 39782 MPa was taken into account. Thus, the assumption of a unique value of the cross sectional second moment of the area I_{exact} (midspan cross section) was correct for the aim of this study. The aforementioned FE analysis was additionally used to consider the eccentric mass of 1.05 kN composed of load cell, steel transition part and steel plate (Fig. 3(b)) at the beam ends, respectively. Similarly, the obtained fundamental frequency does not vary with respect to the analytical models (Eqs. (2)-(3)).

4. Prestress force effect on the deflection shape based on three-point bending tests

4.1 Analytical model

A point load F at the midspan is applied to the static deflection curve $v^{(0)}$ of the simply supported beam in Fig. 6.

By substituting the bending moments in the left- and right-portions of the beam in Fig. 8, Eqs. (2(a)-(b)) reported in Bonopera *et al.* (2018c), in the expression for the curvature of the beam axis $M = -EI_{exact}\, d^2v^{(1)}/dx^2$ yields the solution $v^{(1)} = v^{(0)} + v_{\mathrm{tot}}^{(a)}$. Specifically, $v_{\mathrm{tot}}^{(a)}$ is the deflection curve of the beam under the concentric compressive axial load $N_{x,aver}$ and load F (Fig. 9) (Timoshenko and Gere 1961, Bazant and Cedolin 1991, Tullini 2013) expressed as follows

$$v_{\mathrm{tot}}^{(a)}(x)=\frac{\psi}{2\sqrt{n_{x,aver}}^{\,3}}\left[\frac{1}{\cos\sqrt{n_{x,aver}}\big/2}\sin\left(\sqrt{n_{x,aver}}\,\frac{x}{L}\right)-\sqrt{n_{x,aver}}\,\frac{x}{L}\right]\quad\text{for}\quad 0\le x\le L/2, \tag{4a}$$

$$v_{\mathrm{tot}}^{(a)}(x)=\frac{\psi}{2\sqrt{n_{x,aver}}^{\,3}}\left\{\frac{1}{\cos\sqrt{n_{x,aver}}\big/2}\sin\left[\sqrt{n_{x,aver}}\left(1-\frac{x}{L}\right)\right]-\sqrt{n_{x,aver}}\left(1-\frac{x}{L}\right)\right\}\quad\text{for}\quad L/2\le x\le L, \tag{4b}$$

where $n_{x,aver} = N_{x,aver}\, L^2/\, EI_{exact}$ and $\psi = FL^3/\, EI_{exact}$. As n approaches zero, the limit of Eqs. (4) yields the corresponding first-order displacement $v_{\mathrm{I}}^{(a)}$ expressed as follows

$$v_{\mathrm{I}}^{(a)}(x)=\frac{\Psi}{12}\frac{x}{L}\left[\frac{3}{4}-\left(\frac{x}{L}\right)^2\right]\quad\text{for } 0\le x\le L/2, \tag{5a}$$

$$v_{\mathrm{I}}^{(a)}(x)=\frac{\Psi}{12}\left(1-\frac{x}{L}\right)\left[\frac{2x}{L}-\left(\frac{x}{L}\right)^2-\frac{1}{4}\right]\quad\text{for } L/2\le x\le L. \tag{5b}$$

The vertical displacement $v_{\mathrm{tot}}^{(a)}(x)$ in Eqs. (4) is well approximated by the first-order deflection $v_{\mathrm{I}}^{(a)}(x)$ in Eqs. (5) multiplied by the magnification factor 1 / (1 – $N_{x,aver}$ / N_{crE}) based on the compression-softening theory (Timoshenko and Gere 1961, Bazant and Cedolin 1991)

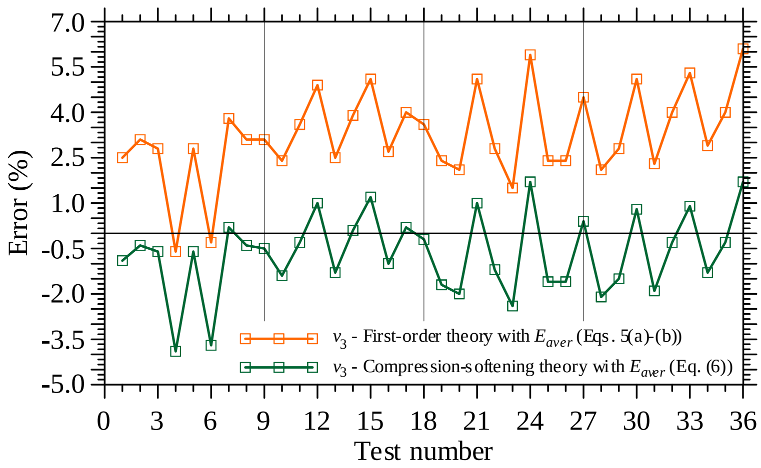

Fig. 10 Errors of displacements v_3 versus test number adopting elastic modulus E_{aver} for all thirty-six test cases

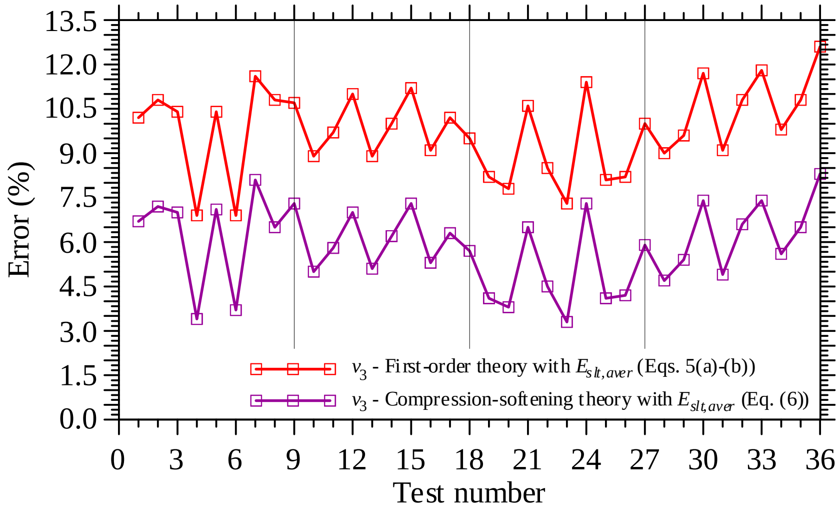

Fig. 11 Errors of displacements v_3 versus test number adopting elastic modulus $E_{slt,aver}$ for all thirty-six test cases

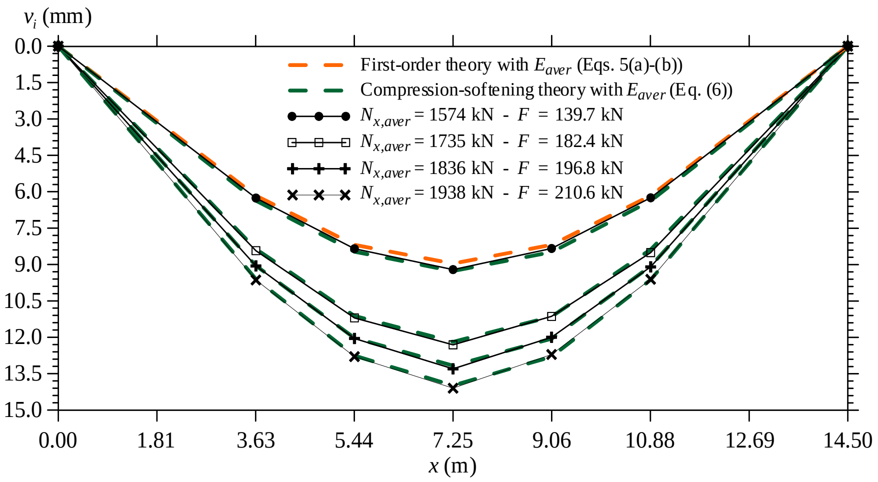

Fig. 12 Comparison of the deflection shapes of the four prestress forces $N_{x,aver}$ for the maximum values of F

$$v_{\mathrm{tot}}^{(x)}(x) = \frac{v_{\mathrm{I}}^{(a)}(x)}{1 - N_{x,aver} / N_{\mathrm{crE}}}, \tag{6}$$

where Euler buckling load is $N_{\mathrm{crE}} = \pi^2 EI_{exact} / L^2$. Thus, the magnification factor coincides with the ratio $v_{\mathrm{I}}^{(a)}(x) / v_{\mathrm{tot}}^{(x)}(x)$.

The measured displacements v_i in the three-point bending tests, presented in Section 2.3, were compared with the analytical displacements obtained by Eqs. (5(a)-(b)) and (6). More details of the formulas reported in this section are described in Bonopera *et al.* (2018c).

4.2 Three-point bending tests and comparison with analytical model

Twelve test cases were defined, yielding a total of thirty-six test combinations (Section 2.3). A good repeatability was experienced. In fact, errors lower than 5.0% were obtained between the reciprocal measurements v_i (Fig. 4). A FE analysis that used 9 beam elements adopting exact shape functions describing second-order effects (Bazant and Cedolin 1991) was employed to determine the buckling loads N_{crE} in Eq. (6). Fig. 10 shows the errors of displacements v_3 through the comparison with the corresponding analytical values $v_{\mathrm{I}}^{(a)}(L/2)$ (Eqs. (5(a)-(b)) and $v_{\mathrm{tot}}^{(x)}(L/2)$ (Eq. (6)) for all thirty-six test cases. Specifically, the errors for the compression–softening theory were computed using the prestress forces $N_{x,aver}$ in Eq. (6).

Fig. 10 indicates that the errors between analytical $v_{\mathrm{tot}}^{(x)}(L/2)$ and measured displacements v_3 were of –3.9% and –3.7% for the nine tests when $N_{x,aver}$ = 1574 kN was applied. The remaining errors were lower than 2.5% (in absolute value). The scattered values obtained by the comparison with the first-order displacements $v_{\mathrm{I}}^{(a)}(L/2)$ are clearly depicted. Specifically, the two functions can be overlapped through a vertical shift, in fact, they differ of the magnification factor. The maximum prestress force $N_{x,aver}$ = 1938 kN was 4.3% of N_{crE}. Consequently, first-order displacements $v_{\mathrm{I}}^{(a)}(L/2)$ were increased by a magnification factor of $1 / (1 - 1938 / 47036) = 1.043$. The magnification factor formula (Eq. (6)) can satisfactorily compute the displacements v_3. Thus, with small magnification factor, the prestress force still seems to be considered as an external compressive load (Fig. 6). Notably, the cables were always in contact with the surrounding metallic duct during testing.

The aforementioned calibration was also executed by adopting the elastic modulus referring to the maximum stresses occurred during the three-point bending test, in accordance with the identification procedure of the elastic modulus $E_{fvt,aver}$ estimated during vibration testing (Section 2.4). These additional elastic moduli were labeled as $E_{slt,aver}$. Specifically, the average reference elastic modulus was $E_{slt,ref}$ = 39525 MPa. Fig. 11 shows that the average errors between analytical and measured displacements v_3 were respectively of 9.8% and 5.9% for the first-order and compression-softening theory. It is confirmed that the correct elastic modulus of static testing on PCI beams is the modulus E obtained through compression tests and assuming σ_2 equal to the 40% of the concrete characteristic strength f_{ck} in Eq. (1) (Bonopera *et al.* 2018c). Notably, the ratio E_{ref} / $E_{slt,ref}$ = 37166 / 39525 = 0.94 agrees with the ratio between secant and dynamic elastic modulus of reinforced concrete beams, where the dynamic modulus is determined through transverse vibration tests on the beams (Jerath and Shibani 1984). Finally, Fig. 12 displays good agreement between the analytical and measured deflection shapes of the four prestress forces $N_{x,aver}$ and corresponding maximum loads F applied (Table 1).

5. Conclusions

A testing program on a large-scale PCI beam with an eccentric straight unbonded tendon was conducted to study the prestress force influence on the fundamental frequency and deflection shape. In these beams, second-order effects are usually lower than 10% of N_{crE}. A range of second-order effects lower than 4.5% of N_{crE} was thus induced in the experiments. Notably, this study also enriches the limited laboratory testing on large-scale prestressed concrete beams. The following conclusions can be drawn within the limitations of the research:

1. It is better to consider the initial elastic modulus of concrete $E_{fvt,aver}$ for simulating free vibrations of PCI beams because the maximum stress due to vibrations is much lower than that by 40% of f_{ck}.
2. The correct elastic modulus for three–point bending test on PCI beams is the secant elastic modulus of concrete E_{aver}.
3. The fundamental frequency is sensitive to the variation of the square root of the elastic modulus of concrete with time. The small increment of the aforementioned parameter was registered in correspondence of a variation of the elastic modulus E_{aver} of 0.8%. No variation with time occurred for the elastic modulus $E_{fvt,aver}$, see Table 2. Specifically, with respect to the study of Jaiswal (2008), a reliable time-dependent elastic modulus evaluation was conducted.
4. The fundamental frequency is unaffected by the prestress force. A variation of the frequency of 1.1% was obtained within a variation of the prestress force of 22.9%. In previous studies (Kim *et al.* 2003, Kim *et al.* 2004, Capozucca 2008, Law *et al.* 2008, Bu and Wang 2011, Xu and Sun 2011, Li *et al.* 2013, Shi *et al.* 2014), efforts were made to use natural frequencies as indicators for predicting the prestress loss in concrete members, where second-order effects were of approximately 5-6%. Nonetheless, the fundamental frequency is confirmed to be an unsuitable indicator for prestress loss detection in PCI beams, as indicated by the analytical study of Jaiswal (2008). The variation of the frequency is caused by the variation of the elastic modulus of concrete with time.
5. The relationship between prestress force and fundamental frequency is well described by the first-order Euler-Bernoulli beam theory (Young and Budynas 2002), considering the variation of the square root of elastic modulus of concrete with time. The small increment of the experimental fundamental frequency of 1.1% may be caused by the increase of the PCI beam's stiffness based on the eccentricity of the tendon (Jaiswal 2008).
6. Vice versa, the relationship between the prestress force and flexural displacements is well described by the magnification factor formula of the compression-softening theory (Timoshenko and Gere 1961, Bazant and Cedolin 1991), even considering the variation of the square root of the elastic modulus of concrete with time.
7. Currently, as reported in the literature review by Noble *et al.* (2015), the reduction of fundamental frequency seems not to be related to the compression-softening theory. Further studies on post-tensioned steel beams will be necessary to take into account for the masses at the end

constraints of the tested specimens, usually composed of load cells and/or loading jacks.

8. Three-point bending tests on post-tensioned concrete specimens under high prestress forces will be conducted to verify the influence of micro-crack closure on the increase in elastic modulus.

Acknowledgments

Experiments were conducted at the National Center for Research on Earthquake Engineering (NCREE) and supported by funding from the National Applied Research Laboratories Project of Taiwan (NCREE-06105C1005). N.T. acknowledges the financial support of the "Research Program FAR 2018" provided by the University of Ferrara. A special gratitude is extended to the technicians of NCREE and students of National Taiwan University, who provided considerable assistance to the authors.

References

ACI 318 (2014), *Building Code Requirements for Structural Concrete and Commentary*, American Concrete Institute, Farmington Hills, Michigan, U.S.A.

Annual Book of ASTM Standards (2016), *Section 4: Construction vol. 04.02. Concrete & Aggregates*, American Society for Testing & Materials.

Bazant, Z.P. and Cedolin, L. (1991), *Stability of Structures*, Oxford University Press, New York, U.S.A.

Bonopera, M., Chang, K.C., Chen, C.C., Lin, T.K. and Tullini, N. (2018a), "Compressive column load identification in steel space frames using second-order deflection-based methods", *Int. J. Struct. Stab. Dyn.*, **18**(7), 1850092.

Bonopera, M., Chang, K.C., Chen, C.C., Lee, Z.K. and Tullini, N. (2018b), "Axial load detection in compressed steel beams using FBG-DSM sensors", *Smart Struct. Syst.*, **21**(1), 53-64.

Bonopera, M., Chang, K.C., Chen, C.C., Sung, Y.C. and Tullini, N. (2018c), "Feasibility study of prestress force prediction for concrete beams using second-order deflections", *Int. J. Struct. Stab. Dyn.*, **18**(10), 1850124.

Bu, J.Q. and Wang, H.Y. (2011), "Effective pre-stress identification for a simply supported PRC beam bridge by BP neural network method", *J. Vibr. Shock*, **30**(12), 155-159.

Capozucca, R. (2008), "Detection of damage due to corrosion in prestressed RC beams by static and dynamic tests", *Constr. Build. Mater.*, **22**(5), 738-746.

Hamed, E. and Frostig, Y. (2006), "Natural frequencies of bonded and unbonded pre-stressed beams pre-stress force effects", *J. Sound Vibr.*, **295**(1-2), 28-39.

Haque, M.N. and Kayali, O. (1998), "Properties of high-strength concrete using a fine fly ash", *Cement Concrete Res.*, **28**(10), 1445-1452.

Hop, T. (1991), "The effect of degree of prestressing and age of concrete beams on frequency and damping of their free vibration", *Mater. Struct.*, **24**(3), 210-220.

Jacobs, S. and De Roeck, G. (2003), "Dynamic testing of a pre-stressed concrete beam", *Proceedings of the 6th National Congress on Theoretical and Applied Mechanics*.

Jaiswal, O.R. (2008), "Effect of prestressing on the first flexural natural frequency of beams", *Struct. Eng. Mech.*, **28**(5), 515-524.

Jerath, S. and Shibani, M.M. (1984), "Dynamic modulus for reinforced concrete beams", *J. Struct. Eng.*, **110**(6), 1405-1410.

Kim, J.T., Ryu, Y.S. and Yun, C.B. (2003), "Vibration based method to detect pre-stress loss in beam type bridges", *Proceedings of the Smart Systems and Non-Destructive Evaluation for Civil Infrastructures*.

Kim, J.T., Yun, C.B., Ryu, Y.S. and Cho, H.M. (2004), "Identification of prestress-loss in PSC beams using modal information", *Struct. Eng. Mech.*, **17**(3-4), 467-482.

Law, S.S. and Lu, Z.R. (2005), "Time domain responses of a pre-stressed beam and pre-stress identification", *J. Sound Vibr.*, **288**(4-5), 1011-1025.

Law, S.S., Wu, S.Q. and Shi, Z.Y. (2008), "Moving load and pre-stress identification using wavelet based method", *J. Appl. Mech.*, **75**(2), 021014.

Li, H., Lv, Z. and Liu, J. (2013), "Assessment of pre-stress force in bridges using structural dynamic responses under moving vehicles", *Math. Probl. Eng.*, 435939.

Li, J. and Zhang, F. (2016), "Experimental research and numerical simulation of influence of pre-stress values on the natural vibration frequency of concrete simply supported beams", *J. Vibroeng.*, **18**(7), 4592-4604.

Limongelli, M.P., Siegert, D., Merliot, E., Waeytens, J., Bourquin, F., Vidal, R., Le Corvec, V., Gueguen, I. and Cottineau, L.M. (2016), "Damage detection in a post tensioned concrete beam-experimental investigation", *Eng. Struct.*, **128**, 15-25.

Lu, Z.R. and Law, S.S. (2006), "Identification of pre-stress force from measured structural responses", *Mech. Syst. Sign. Proc.*, **20**(8), 2186-2199.

Miyamoto, A., Tei, K., Nakamura, H. and Bull, J.W. (2000), "Behavior of pre-stressed beam strengthened with external tendons", *J. Struct. Eng.*, **126**(9), 1033-1044.

Noble, D., Nogal, M., O'Connor, A. and Pakrashi, V. (2015), "Dynamic impact testing on post-tensioned steel rectangular hollow sections; an investigation into the "compression-softening" effect", *J. Sound Vibr.*, **355**, 246-263.

Noble, D., Nogal, M., O'Connor, A. and Pakrashi, V. (2016), "The effect of prestress force magnitude and eccentricity on the natural bending frequencies of uncracked prestressed concrete beams", *J. Sound Vibr.*, **365**, 22-44.

Noh, M.H., Seong, T.R., Lee, J. and Park, K.S. (2015), "Experimental investigation of dynamic behavior of prestressed girders with internal tendons", *Int. J. Steel Struct.*, **15**(2), 401-414.

Ortega, N.F., Moro, J.M. and Meneses, R.S. (2018), "Theoretical model to determine bond loss in prestressed concrete with reinforcement corrosion", *Struct. Eng. Mech.*, **65**(1), 1-7.

Palanisamy, S.P., Maheswaran, G., Annaamalai, M.G.L. and Vennila, P. (2015), "Steel slag to improve the high strength of concrete", *Int. J. Chemtech Res.*, **7**(5), 2499-2505.

Rebecchi, G., Tullini, N. and Laudiero, F. (2013), "Estimate of the axial force in slender beams with unknown boundary conditions using one flexural mode shape", *J. Sound Vibr.*, **332**(18), 4122-4135.

Saiidi, M., Douglas, B. and Feng, S. (1994), "Prestress force effect on vibration frequency of concrete bridges", *J. Struct. Eng.*, **120**(7), 2233-2241.

Shi, L., He, H. and Yan, W. (2014), "Pre-stress force identification for externally pre-stressed concrete beam based on frequency equation and measured frequencies", *Math. Probl. Eng.*, 840937.

Timoshenko, S.P. and Gere, J.M. (1961), *Theory of Elastic Stability*, McGraw-Hill, New York, U.S.A.

Tullini, N. and Laudiero, F. (2008), "Dynamic identification of beam axial loads using one flexural mode shape", *J. Sound Vibr.*, **318**(1-2), 131-147.

Tullini, N., Rebecchi, G. and Laudiero, F. (2012), "Bending tests to estimate the axial force in tie-rods", *Mech. Res. Commun.*, **44**, 57-64.

Tullini, N. (2013), "Bending tests to estimate the axial force in slender beams with unknown boundary conditions", *Mech. Res. Commun.*, **53**, 15-23.
Wang, T.H., Huang, R. and Wang, T.W. (2013), "The variation of flexural rigidity for post-tensioned prestressed concrete beams", *J. Mar. Sci. Technol.*, **21**(3), 300-308.
Xu, J. and Sun, Z. (2011), "Pre-stress force identification for eccentrically pre-stressed concrete beam from beam vibration response", *Tech. Sci. Press*, **5**(2), 107-115.
Young, W.C. and Budynas, R.G. (2002), *Roark's Formulas for Stress and Strain*, McGraw-Hill.
Zhang, Y. and Li, R. (2007), "Natural frequency of full-prestressed concrete beam", *Trans. Tianjin Univ.*, **13**(5), 354-359.

CC